1-DOF Dynamic Pitching Robot that Independently Controls Velocity, Angular Velocity, and Direction of a Ball

Wataru Mori*, Jun Ueda*+, Tsukasa Ogasawara*

* *Graduate School of Information Science, Nara Institute of Science and technology, Japan. ogasawar@is.naist.jp*

+ *Mechanical Engineering, Georgia Institute of Technology, Atlanta, GA., U.S.A. jun.ueda@me.gatech.edu*

Abstract

This paper demonstrates that a 1-DOF planar ball-throwing robot has the capability of controlling three kinematic variables of a ball independently: translational velocity, angular velocity, and direction. The throwing motion is modeled using two underactuated contact dynamics, called a finger-link contact model and a fingertip contact model, with a unidirectional transition from one model to another. A combination of a preliminary global search method and a search algorithm based on a simulated annealing (SA) algorithm provides joint torque commands for this highly nonlinear system. An experimental system with a 1-DOF planer manipulator has been developed that throws a disk (ball) in a frictionless plane. The experimental results confirm the validity of the contact models and the feasibility of independent control of the three kinematic variables.

keywords: Dynamic manipulation, Pitching, Contact model, Motion planning

1 Introduction

Dynamic manipulation is an actively studied area in robotics that deals especially with the investigation and acquisition of manipulation skills induced by the dynamic interaction between a robot and an object [1, 2, 3]. The results presented by Lynch et al. [4, 5] are remarkable in showing the various manipulations of a rectangular object, such as throwing and rotation on a link that can be realized by a robot having relatively low degrees of freedom (DOF). In these works, the nonholonomic property of the dynamics plays an important role in achieving tasks even though the systems are underactuated.

This paper discusses a ball-throwing motion by a robotic-link mechanism. Several groups have studied ball-throwing robots [6, 7, 8, 9]. However, the main aim was the control of the trajectory of a ball, i.e., the velocity and direction. Consider the ball-throwing motion of humans. As illustrated in Fig. 1, for example, pitching a ball in baseball is considered complex since not only the velocity of the ball needs to be controlled appropriately, but also the direction and angular velocity. In biomechanics, a more accurate investigation including the motion of fingers has been conducted, e.g., [10].

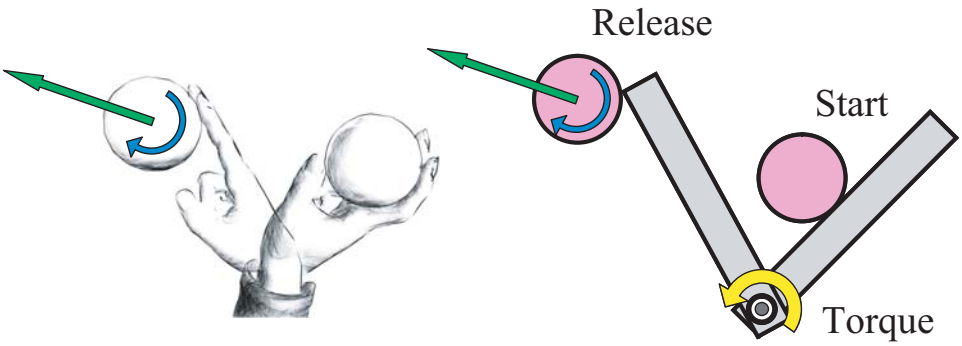

Figure 1: Ball Pitching Motion

The goal of this work is to independently control three kinematic variables of a ball released from a robot link: velocity, angular velocity, and direction, starting from a common initial condition. All three kinematic variables are determined by the physical interaction between the ball and hand in a very short period of time from the start of the motion to the release of the ball where the interaction is fundamentally dynamic. The contact condition between the ball and hand just before the release is particularly important and is regarded as *nonprehensile*, i.e., not under a static grasping condition, where a limited number of fingers are in contact with the ball, dynamically applying force or torque to the ball.

This paper considers a simple, planar robot that uses a 1-DOF link to throw a disk in a horizontal plane. We show that the condition of contact between the robot finger and ball transits from one underactuated contact model, named a 'finger-link contact model', to another underactuated contact model, named a 'fingertip contact model', during the motion. This paper presents preliminary results of numerical simulation and experiments on the capability of controlling the three kinematic variables independently. A numerical algorithm to acquire joint torque commands is developed by applying a simulated annealing (SA) method. The validity of the contact models is confirmed by experiments. Experimental results indicate that the independent control on the three kinematic variables is feasible.

2 Experimental System

Figure 2 shows the experimental system developed for this study. To simplify the problem, throwing motion in the horizontal plane is considered. The planar manipulator has a single DOF swing-arm mechanism driven by a DC motor. A plastic disk (hereafter called a *ball*) is used instead of a 3-dimensional ball. The friction between the ball and the link is assumed high enough so that the ball rolls on the link surface without slip because of anti-skid rubber attached on the link. To eliminate the friction between the ball and the floor an air table is used. Therefore, we assume that the velocity, angular velocity, and direction never change after the release. A search algorithm described later and applied to the DC motor generates the torque command to the joint. The stopper attached to the link is used to set a constant initial condition between the link and the disk. As shown in Fig. 3, the ve-

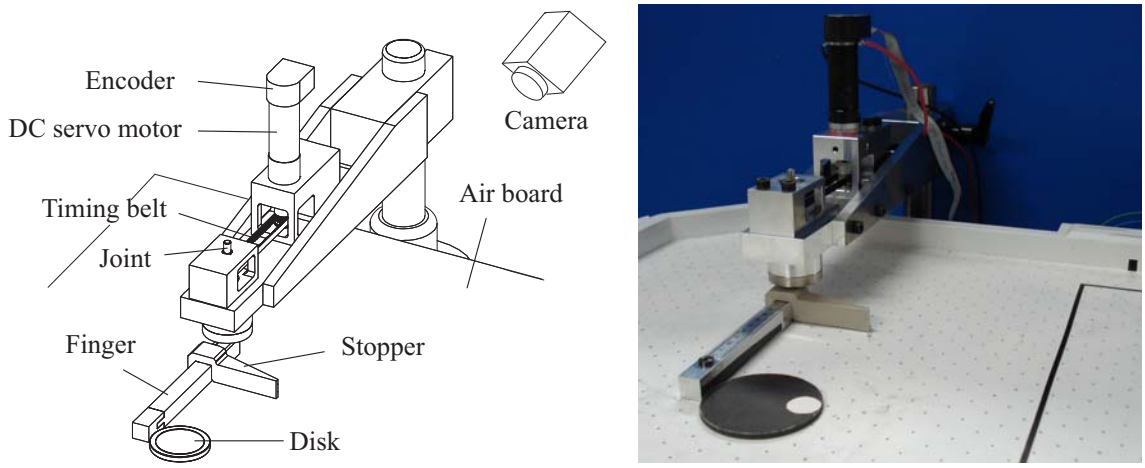

Figure 2: Experimental Setup: 1 DOF Planar Ball-throwing Robot

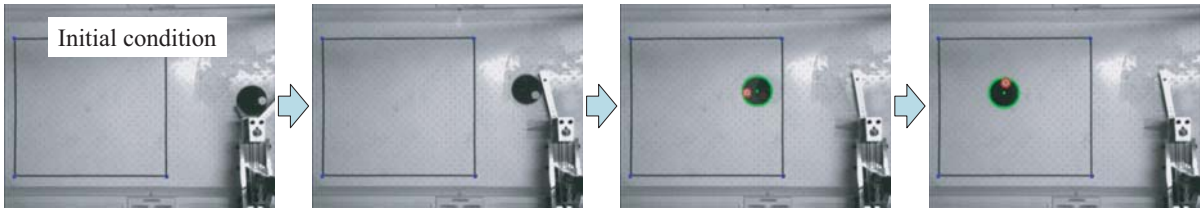

Figure 3: Measurement of Velocity, Angular Velocity, and Direction of the Ball : Snapshots of Image Processing

locity, angular velocity, and direction of the ball after the release from the link are measured by image processing using a camera. The dimensions and physical parameters are shown in Table 2.

3 Contact Model between Robot finger and Ball

3.1 Contact Models and Transition

Two dynamic models are presented based on the condition of contact between the ball and robot link: (1) the finger-link contact model, and (2) the fingertip contact model. The finger-link contact model shown in Fig. 4 represents the dynamics where the ball and link keep a rolling contact condition. The fingertip contact model shown in Fig. 5 represents the dynamics where the ball is in contact with an edge of the link (fingertip).

The relationship between the two contact models is illustrated in Fig. 6. The finger-link contact model is initially applied since the initial condition (see the most-left image in Fig. 3) is given under this condition. The ball is released from the link if the contact force f_{lh} acting on the ball from the link becomes zero. In this paper we don't discuss the case where the link contacts again with a ball once released. If the ball rolls up along the surface of the link keeping a rolling contact, and reaches the end of the link, then the condition of contact transits to the fingertip contact model. This transition is

Parameter	Value
Mass of Finger m_1	96.0 [g]
Mass of Disk m_2	7.5 [g]
Length of Finger L	152.5 [mm]
Width of Finger d	15 [mm]
Distance between Joint and COG of Finger r_{g1}	72.5 [mm]
Radious of Disk r	36.5 [mm]
Initial finger angle θ_0	$\frac{\pi}{4}$ [rad]
Initial displacement of Disk ℓ_0	60 [mm]

Table 1: Specifications of experimental system

unidirectional and never goes back to the finger-link contact model. Similarly, the ball is released from the fingertip if the contact force f_f acting on the ball from the link becomes zero.

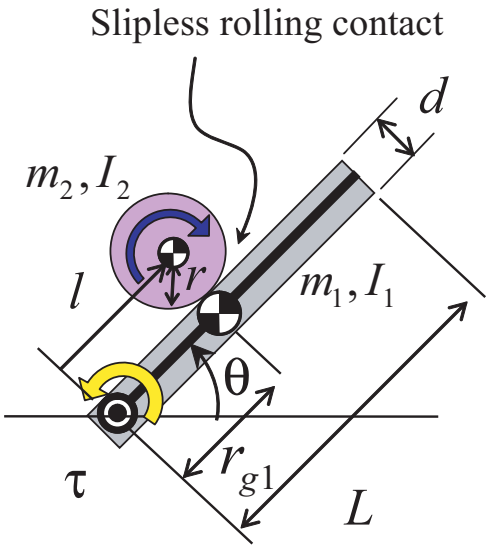

Figure 4: Finger-link contact model

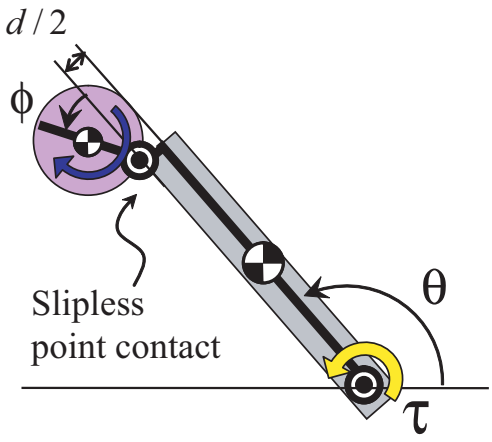

Figure 5: Fingertip contact model

3.2 Dynamic Equation

3.2.1 Finger-link contact model

The dynamic equation of the finger-link contact model is given as follows.

$$\begin{bmatrix} \tau \\ 0 \end{bmatrix} = \begin{bmatrix} M_{11} & M_{12} \\ M_{21} & M_{22} \end{bmatrix} \begin{bmatrix} \ddot{\theta} \\ \ddot{\ell} \end{bmatrix} + \begin{bmatrix} h_1 \\ h_2 \end{bmatrix} \tag{1}$$

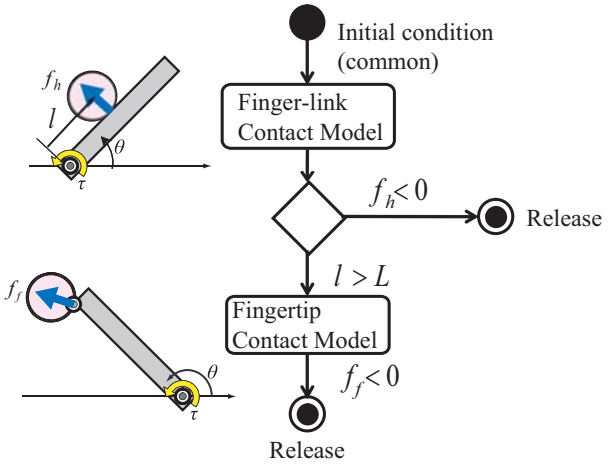

Figure 6: Transition of the Condition of Contact

$$M_{11} = m_1 r_{g1}^2 + m_2 \left(r^2 + \frac{1}{4} d^2 + r d_1 + \ell^2 \right) + I_1 + I_2 \tag{2a}$$

$$M_{12} = -m_2 \left(r - \frac{1}{2} d \right) - \frac{I_2}{r} \tag{2b}$$

$$M_{21} = -m_2 \left(r - \frac{1}{2} d \right) - \frac{I_2}{r} \tag{2c}$$

$$M_{22} = m_2 + \frac{I_2}{r^2} \tag{2d}$$

$$h_1 = 2 m_2 \ell \dot{\theta} \dot{\ell} \tag{2e}$$

$$h_2 = -m_2 \ell \dot{\theta}^2 \tag{2f}$$

where θ is the angle of the link joint, ℓ is the translational displacement of the ball along the longitudinal direction of the link, and τ is the joint torque. m_1 and m_2 denote the masses, and I_1 and I_2 denote the moment of inertia of the link and ball respectively. L is the length, and d is the width of the link. r_{g1} is the distance from the center of the joint to the center of gravity of the link. Assume that the shape of the ball is a perfect circle where r is the radius.

When the ball is released directly from the finger-link contact model without the transition to the fingertip model, three kinematic variables, i.e., the velocity v, angular velocity ω, and direction d_b, of the ball are given as follows.

$$v = \sqrt{\dot{\ell_r}^2 + \ell_r^2 \dot{\theta_r}^2 + r^2 \dot{\theta_r}^2 - 2 \dot{\ell_r} r \dot{\theta_r}} \tag{3a}$$

$$d_b = \arctan \left(\frac{\ell_r \sin\theta_r + \left(\frac{d}{2} + r \right) \cos\theta_r}{\ell_r \cos\theta_r - \left(\frac{d}{2} + r \right) \sin\theta_r} \right) + \pi \tag{3b}$$

$$\omega = \frac{\dot{\ell_r}}{r} - \dot{\theta_r} \tag{3c}$$

where the variables with subscript r denote the quantities at the time of the release.

3.2.2 Fingertip contact model

The dynamic equation for the fingertip contact model is given as follows.

$$\begin{bmatrix} \tau \\ 0 \end{bmatrix} = \begin{bmatrix} M_{11} & M_{12} \\ M_{21} & M_{22} \end{bmatrix} \begin{bmatrix} \ddot{\theta} \\ \ddot{\phi} \end{bmatrix} + \begin{bmatrix} h_1 \\ h_2 \end{bmatrix} \tag{4}$$

$$\begin{aligned}
M_{11} &= m_1 r_{g1}^2 + m_2 (r^2 + \frac{1}{4} d^2 + r d_1 \sin\phi && \text{(5a)} \\
&+ L^2 + 2Lr\cos\theta) + I_1 + I_2 && \text{(5b)} \\
M_{12} &= m_2 \left(Lr\cos\phi + \frac{1}{2} d \sin\phi r + r^2 \right) + I_2 && \text{(5c)} \\
M_{21} &= m_2 \left(Lr\cos\phi + \frac{1}{2} d \sin\phi r + r^2 \right) + I_2 && \text{(5d)} \\
M_{22} &= m_2 r^2 + I_2 && \text{(5e)} \\
h_1 &= m_2 \left(dr\cos\phi - 2Lr\sin\phi \right) \dot{\theta}\dot{\phi} \\
&+ m_2 \left(\frac{1}{2} dr\cos\phi - Lr\sin\phi \right) \dot{\phi}^2 && \text{(5f)} \\
h_2 &= m_2 r \left(L\sin\phi - \frac{1}{2} d\cos\phi \right) \dot{\theta}^2 && \text{(5g)}
\end{aligned}$$

where ϕ is the angle of the center of the ball measured from the point of contact. When the ball is released from the fingertip contact model, the velocity, angular velocity, and direction of the ball are given as follows.

$$\begin{aligned}
v &= \sqrt{X^2 + Y^2} && \text{(6a)} \\
&X = \left(-L\sin\theta_r \dot{\theta}_r - r\sin\left(\theta_r + \phi_r\right) \left(\dot{\theta}_r + \dot{\phi}_r \right) \right)^2 \\
&Y = \left(L\cos\theta_r \dot{\theta}_r + r\cos\left(\theta_r + \phi_r\right) \left(\dot{\theta}_r + \dot{\phi}_r \right) \right)^2 \\
d_b &= \arctan\left(\frac{L\cos\theta_r \dot{\theta}_r + r\cos\left(\theta_r + \phi_r\right) \left(\dot{\theta}_r + \dot{\phi}_r \right)}{-L\cos\theta_r \dot{\theta}_r - r\sin\left(\theta_r + \phi_r\right) \left(\dot{\theta}_r + \dot{\phi}_r \right)} \right) + \pi && \text{(6b)} \\
\omega &= \dot{\phi}_r - \dot{\theta}_r && \text{(6c)}
\end{aligned}$$

The two contact models are underactuated since each of the dynamic equations includes two variables but only one torque input. In addition, the two models are second-order nonholonomic systems since both of the models satisfy the condition proposed by Nakamura and Oriolo [11].It should be noted that the transition from the finger-link contact to fingertip contact does not necessarily happen as shown in Fig. 6; the ball may be released directly from the finger-link contact in a certain throwing movement. The combination of throws with and without the transition is expected to realize a wider range of kinematic variables than assuming a single contact model model.

4 Acquisition of Joint Torque

4.1 Problem Statement

This paper investigates the control capability of the ball in terms of v, d_b, and ω starting from the same initial condition. Since the dynamics is highly nonlinear and underactuated, numerical methods are used for preliminary investigation. The goal is to obtain joint torque commands that change any one of the three kinematic variables of interest, but keep the remaining one or two variables unchanged.

4.2 Joint Torque Command using Radial Basis Functions

Radial Basis Functions (RBF) [12] are applied to represent a time function of joint torque as follows.

$$\tau(t) = \sum_{i=1}^{4} w_i \Psi_i \tag{7}$$

where Ψ_i is a RBF defined by

$$\Psi_i = \exp\left(-\frac{1}{2\sigma_i^2} (t - c_i)^2 \right). \tag{8}$$

In this paper, we consider joint torque from 0.0 [s] $\sim$ 1.0 [s] given by the summation of 4 weighted RBFs. To reduce the dimension of search space for generating joint torque commands, $c_1 = 2/7$, $c_2 = 3/7$, $c_3 = 4/7$, $c_4 = 5/7$, $\sigma_1 = 0.08$, $\sigma_2 = 0.08$, $\sigma_3 = 0.08$, and $\sigma_4 = 0.08$ are given in advance. Therefore, only the weights, $W = [w_1, w_2, w_3, w_4]$, are free parameters. Expansion of the search area by freeing the parameters currently fixed including the number of RBFs will be conducted in a future paper.

4.3 Preliminary Global Search and Simulated Annealing

First, a preliminary global search for $W = [w_1, w_2, w_3, w_4]$ is performed. The range of individual parameters is determined as $0.0 \leqq w_1 \leqq 1.0$, $-1.0 \leqq w_{2,3,4} \leqq 1.0$ and the normal step size is set to 0.1. The step size is decreased to 0.01 for $0.0 \leqq w_1 \leqq 0.1$ and $-0.1 \leqq w_{2,3,4} \leqq 0.1$. The velocity, angular velocity, and direction for each torque command is calculated using MATLAB simulation and the result is plotted in a 3-dimensional graph as shown in Fig. 7 (a).

Next, to find a torque command that realizes a particular set of kinematic variables of the ball, a search algorithm based on simulated annealing (SA) [13] is applied using the following criterion function.

$$J = K_v |v_d - v| + K_d |d_d - d_b| + K_\omega |\omega_d - \omega| \tag{9}$$

where K_v=100.0, K_d=10.0, and K_ω=0.1 are weights. v_d, d_d, and ω_d are desired variables for v, d_b, and ω respectively. Optimization of J obtains $W = [w_1, w_2, w_3, w_4]$ that realizes the desired kinematic variables. The initial condition for SA is chosen from the closest ones obtained by the global search.

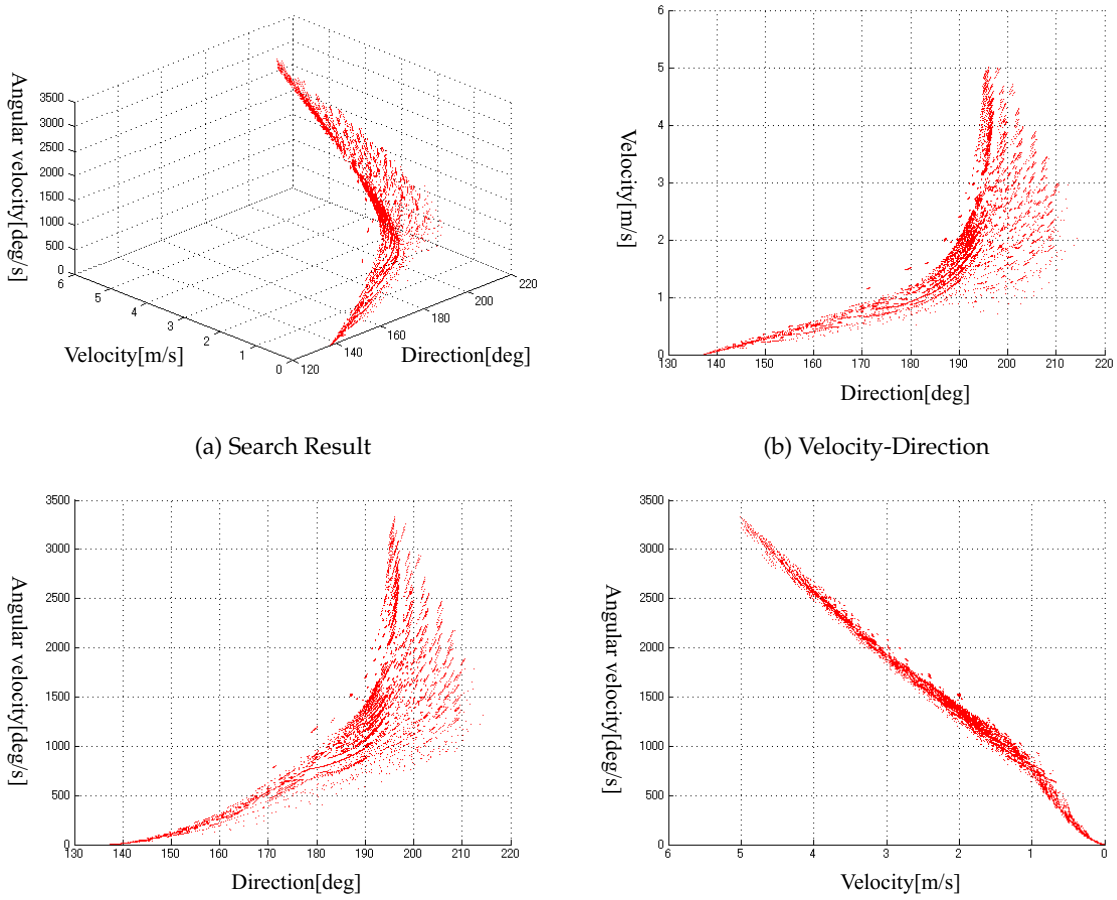

(a) Search Result

(b) Velocity-Direction

(c) Angular velocity-Direction

(d) Angular velocity-Velocity

Figure 7: Result of Preliminary Global Search

4.4 Feasibility of Independent Control on Two Kinematic Variables

Figure 7 shows the result of preliminary global search. Figure 7 (b)-(d) shows the distributions of the results in terms of two out of three kinematic variables. Figure 7(b) shows the distribution of the results in a velocity-direction plane, indicating that the independent control in terms of velocity and direction is feasible when neglecting angular velocity. For example, points A to C in Fig. 8 obtain the same velocity but different directions. Also, points C to E obtain the same direction but different velocities. Fig. 7(c) indicates that the independent control in terms of angular velocity and direction is feasible when neglecting velocity. In contrast, Fig. 7(d) shows that the velocity and angular velocity are strongly correlated. This strong correlation is reasonable since, e.g., as can be seen in (3a) and (3c), the only factor that makes (3a) independent from (3c) is ℓ_r which appears in the second term of (3a), i.e., $\dot{\ell}_r$ and $\dot{\theta}_r$ are included in both (3a) and (3c). Without ℓ_r, (3a) is totally dependent on (3c). In other words, the independent control in terms of velocity and angular velocity neglecting direction is still feasible even though the range is small.

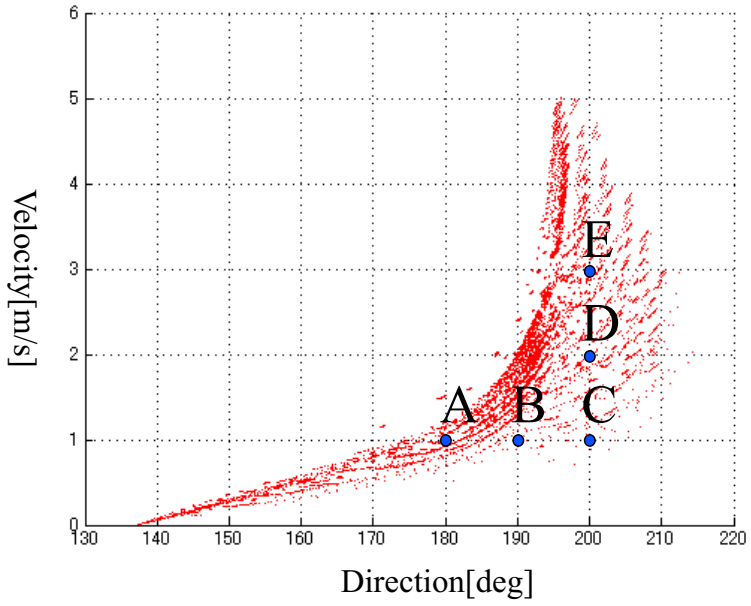

Figure 8: Independent control of Velocity and Direction

4.5 Feasibility of Independent Control on Three Kinematic Variables

Figure 9 shows a basic concept of the independent control. Taking the horizontal axis on velocity for example, the independent control in terms of velocity is to find torque commands corresponding to the two points along the horizontal axis from a base point. The difference among the three throws on the horizontal axis is only on velocity. The remaining two values, angular velocity and direction, are unchanged.

Set a base point that achieves the velocity of 1.23[m/s], direction of 195.0[deg], and angular velocity of 868.4[deg/s]. Joint torques for Throws 1 to 6 shown in the figure have been obtained using the SA method. Table 3 shows the obtained kinematic variables. As shown in the table, the independent control in terms of the three kinematic variables is considered feasible even though the range is small. We would like to emphasize that the main focus of this paper is to demonstrate the feasibility of independent control which we believe has been shown by the observation of the Throws 1–6. This small range may be due to the choice of parameters of the RBFs. A different torque generation method might produce a wider range that will be explored in the future work.

Table 2: Comparison between Simulation and Experiment for Throws A – E

		Velocity [m/s]	Direction [deg]	Angular velocity [deg/s]
A	Simulation	1.00	**179.9**	855.8
	Experiment	1.07	183.5	810.8
	Error [%]	6.9	2.0	5.3
B	Simulation	1.00	**190.0**	659.0
	Experiment	0.94	191.4	611.9
	Error [%]	6.1	0.7	7.1
C	Simulation	**1.00**	**200.0**	672.9
	Experiment	1.01	200.2	696.5
	Error [%]	1.2	0.1	3.5
D	Simulation	**2.00**	200.1	1385.8
	Experiment	1.90	199.8	1330.3
	Error [%]	4.8	0.1	4.0
E	Simulation	**3.00**	200.0	1886.8
	Experiment	2.59	200.8	1760.9
	Error [%]	13.8	0.4	6.7

5 Experiment 1: Pitching in Horizontal Plane

5.1 Validation of Experimental System: Comparison between MATLAB Simulation and Experiments

Throws A–E are used to validate the simulation models. Subfigures (a) and (b) in the Figures 10 to 14 show the comparisons between the MATLAB simulations using the contact models and experimental results. Not that the ball was released from the finger-link contact state for Trhow E. Table 2 shows the obtained kinematic variables and errors. Overall, the experimental results agree well with the simulation. Subfigure (c) in each of the figures shows the result of the simulated annealing (SA). It shows the magnitude of the criterion function J versus iteration number. The red circle indicates the minimum value of J. Subfigure (d) shows the obtained joint torque command.

5.2 Independent Control of Two Kinematic Variables

As described earlier, Throws A–E have been obtained in the velocity-direction plane, neglecting the change in the angular velocity. Figures 15 and 16 show the comparison among Throws A–C and C–E respectively.

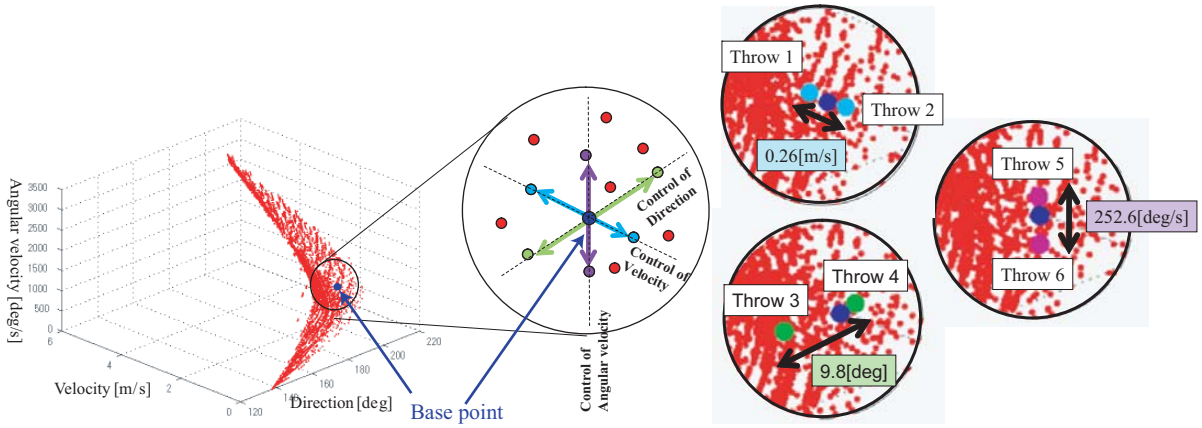

Figure 9: Independent Control of Three Kinematic Variables

Table 3: Independent Control of Three Kinematic Variables (Experiment)

	Velocity [m/s]	Direction [deg]	Angular velocity[deg/s]
Base	1.23	195.0	868.4
Throw 1	**1.35**	194.7	889.8
Throw 2	**1.09**	194.9	880.0
Throw 3	1.22	**188.3**	895.7
Throw 4	1.19	**198.1**	871.8
Throw 5	1.24	194.6	**987.4**
Throw 6	1.22	194.6	**734.8**

5.3 Independent Control of Three Kinematic Variables

Figures 17 to 19 show the experimental results for Throws 1 to 6. For example, Fig. 17 shows the results in terms of velocity by keeping the remaining two variables unchanged. The observation of the experimental results confirms the feasibility of independent control of the three kinematic variables although the range is limited.

6 Experiment 2: Throwing in a Vertical Plane

The presented contact models in the horizontal plane can be easily extended to vertical planes by taking the effect of gravity into account. Figure 21 shows the modified experimental system where an open-top box is used as the goal. Given a position of the goal in an x-y vertical plane, the velocity and direction of the ball at the release are obtained by calculating the ballistic motion of the ball. Figure 20 shows the result of global search by taking the effect of the gravity into account. The SA method is then applied to find the corresponding torque input such that the ball enters the goal. Figures 22 and 23 show successful results for two different cases. Note that the number of trajectories that reach

a particular position of the goal is not unique. The fastest trajectory among the candidates has been chosen in this experiment.

7 Discussion and Conclusion

This paper has demonstrated that a 1-DOF planar-robot-link mechanism has the capability of controlling three kinematic variables of a ball independently: velocity, angular velocity, and direction. Contact dynamics describing the robot throwing, with a transition from finger-link contact to fingertip contact, has been proposed and validated by simulation and experiment. A combination of the global search and the SA algorithm provides joint torque commands for this highly nonlinear dynamic system.

This paper focused on the modeling and preliminary feasibility study on the independent control. As presented, the two contact models are fundamentally underactuated, thus satisfying the nonholonomic property. In addition, the transition from one model to another is unidirectional in this throwing motion. The difference of these throwing dynamics from other underactuated systems is that the contact dynamics switch instead of the controller; the switching-control technique has been used widely in many papers on underactuated systems. This unique characteristic may be a key to controlling the underactuated problem [14]. A detailed mathematical analysis will follow in our future paper.

APPENDIX

A Check of partial integrability

One of the conditions for partial integrability does not hold for the Finger-link contact model (1) and the Fingertip contact model (4) which implies that both of the dynamic models have the second order nonholonomic property. This appdendix briefly examines this condition. According to Oriolo and Nakamura[11], one of the conditions for partial integrability is that the kinetic energy is not dependent on the unactuated joint values, i.e.,

$$\frac{\partial}{\partial q_2}\left(\dot{\boldsymbol{q}}^T \boldsymbol{M} \dot{\boldsymbol{q}}\right) = 0 \tag{10}$$

where $\boldsymbol{M} = \begin{bmatrix} M_{11} & M_{12} \\ M_{21} & M_{22} \end{bmatrix}$. Note that $\boldsymbol{q} = [q_1, q_2]^T = [\theta, \ell]^T$ for the Finger-link contact model) and $\boldsymbol{q} = [q_1, q_2]^T = [\theta, \phi]^T$ for the Fingertip contact model. This condition does not hold for both of the models since:

$$\begin{aligned} \frac{\partial}{\partial q_2}\left(\dot{\boldsymbol{q}}^T \boldsymbol{M} \dot{\boldsymbol{q}}\right) &= \frac{\partial}{\partial \ell}\Big[m_2 \dot{\theta}^2 \ell^2 + \left(I_1 + I_2 + m_2 r^2 + \frac{1}{4} m_2 d^2 + m_2 d r + m_1 r_{g1}^2\right)\dot{\theta}^2 \\ &\quad + \left(-2m_2 r - m_2 d - \frac{2I_2}{r}\right)\dot{\theta}\dot{\ell} + \left(m_2 + \frac{I_2}{r^2}\right)\dot{\ell}^2\Big] \\ &= 2m_2 \dot{\theta}^2 \ell \neq 0 \end{aligned} \tag{11}$$

for the Finger-link contact model given in (1) , and

$$\begin{aligned}\frac{\partial}{\partial q_2}\left(\dot{\boldsymbol{q}}^T \boldsymbol{M}\dot{\boldsymbol{q}}\right) &= \frac{\partial}{\partial \phi}\Big[\left(\left(\dot{\theta}+\dot{\phi}\right) m_2 r d\dot{\theta}\right)\sin\phi + \left(\left(\dot{\theta}+\dot{\phi}\right) 2m_2 r L\dot{\theta}\right)\cos\phi \\ &\quad + \left(I_2 + m_2 r^2\right)\left(\dot{\theta}^2 + 2\dot{\theta}\dot{\phi} + \dot{\phi}^2\right) + \left(\frac{1}{4}m_2 d^2 + m_1 r_{g1}^2 + m_2 L^2 I_1\right)\dot{\theta}^2\Big] \\ &= m_2 r d\dot{\theta}\left(\dot{\theta}+\dot{\phi}\right)\cos\phi - 2m_2 r L\dot{\theta}\left(\dot{\theta}+\dot{\phi}\right)\sin\phi \neq 0 \end{aligned} \tag{12}$$

for the Fingertip contact model given in (4).

REFERENCES

[1] M. Mason and K. Lynch, "Dynamic manipulation," *Proceedings of the 1993 IEEE/RSJ International Conference onIntelligent Robots and Systems, Tokyo, Japan*, vol. 1, 1993.

[2] E. Aboaf, S. Drucker, and C. Atkeson, "Task-level robot learning: juggling a tennis ball more accurately," *Proceedings on the 1989 IEEE International Conference on Robotics and Automation, Scottsdale Az.*, pp. 1290–1295, 1989.

[3] Q. Li and S. Payandeh, "Planning Velocities of Free Sliding Objects as a Free Boundary Value Problem," *The International Journal of Robotics Research*, vol. 23, no. 1, p. 69, 2004.

[4] K. M. Lynch and M. T. Mason, "Dynamic underactuated nonprehensile manipulation," *1996 IEEE/RSJ International Conference on Intelligent Robots and Systems, Osaka, Japan*, pp. 889–896, 1996.

[5] M. T. Mason, "Progress in nonprehensile manipulation," *The International Journal of Robotics Research*, vol. 18, no. 11, pp. 1129–1141, 1999.

[6] E. Aboaf, C. Atkeson, and D. Reinkensmeyer, "Task-Level Robot Learning: Ball Throwing," *AIM-1006*, 1987.

[7] J. Schneider and R. Gans, "Efficient search for robot skill learning: simulation and reality," *Proceedings of the IEEE/RSJ International Conference on Intelligent Robots and Systems, Munich, Germany*, vol. 2, 1994.

[8] N. Kato, K. Matsuda, and T. Nakamura, "Adaptive control for a throwing motion of a 2 DOF robot," *Advanced Motion Control, 1996. AMC'96-MIE. Proceedings., 1996 4th International Workshop on*, vol. 1, 1996.

[9] T. Senoo, A. Namiki, and M. Ishikawa, "High-speed throwing motion based on kinetic chain approach," *Proc. of IEEE/RSJ International Conference on Intelligent Robots and Systems, Nice, France*, pp. 3206–321 153, 2008.

[10] J. Hore, S. Watts, J. Martin, and B. Miller, "Timing of finger opening and ball release in fast and accurate overarm throws," *Experimental Brain Research*, vol. 103, no. 2, pp. 277–286, 1995.

[11] Y. Nakamura and G. Oriolo, "Control of mechanical systems with second-order nonholonomic constraints: Underactuated manipulators," *Proceedings of the 30th IEEE Conference on Decision and Control, Brighton, England*, no. 3, pp. 2398–2403, 1991.

[12] D. B. Martin, *Radial basis functions: theory and implementations*. Cambridge University Press, Cambridge, UK, 2003.

[13] E. Aarts and J. Korst, "Simulated annealing and Boltzmann machines," *IEEE Control Systems Magazine*, vol. 9, pp. 31–37, 1989.

[14] M. W. Spong, "Bipedal locomotion, robot gymnastics, and robot air hockey: A rapprochement," *Super-Mechano Systems (SMS'99) Workshop, Tokyo, Japan*, 1999.

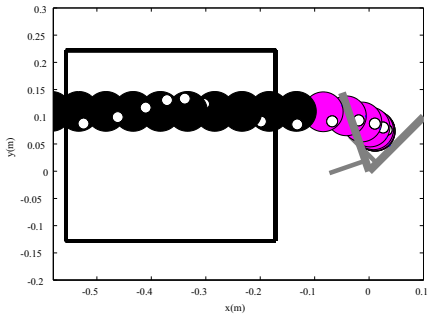

(a) Simulation

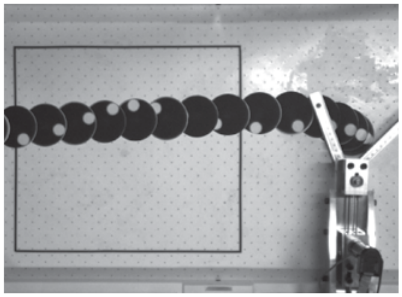

(b) Experiment

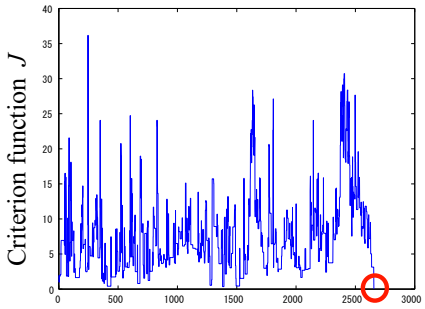

(c) Simulated Annealing

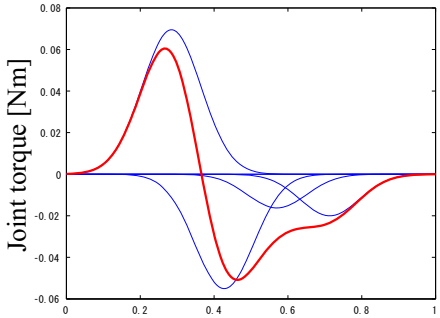

(d) Obtained joint torque

Figure 10: Throw A

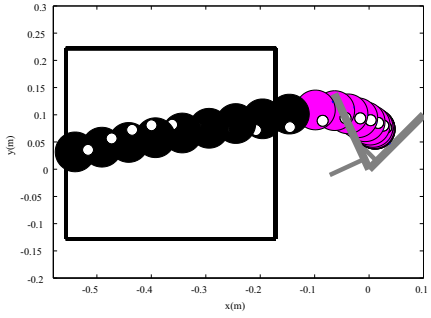

(a) Simulation

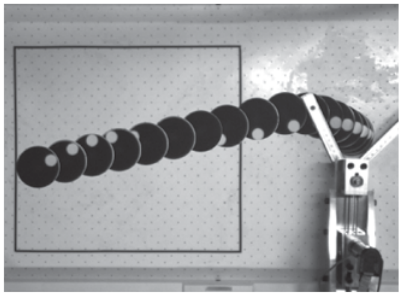

(b) Experiment

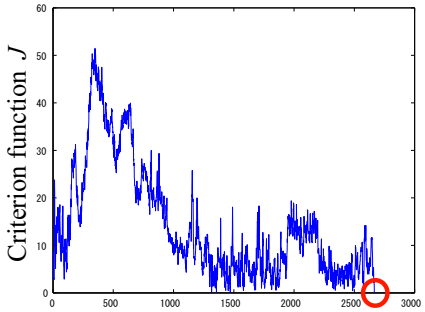

(c) Simulated Annealing

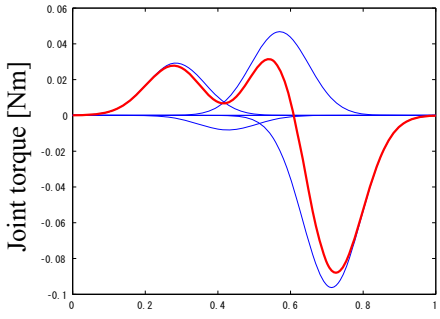

(d) Obtained joint torque

Figure 11: Throw B

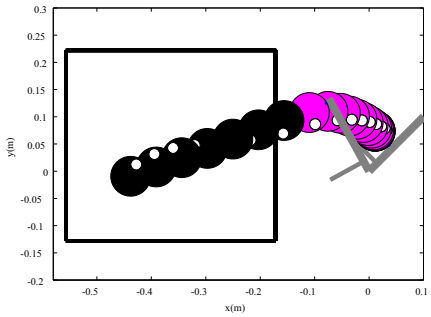

(a) Simulation

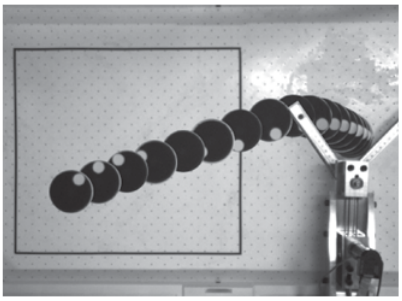

(b) Experiment

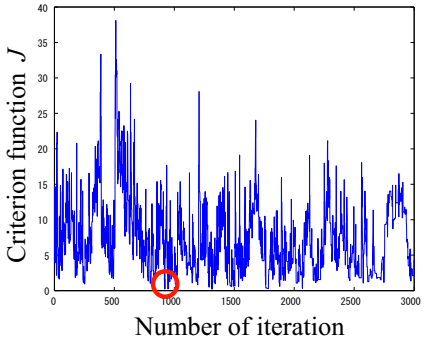

(c) Simulated Annealing

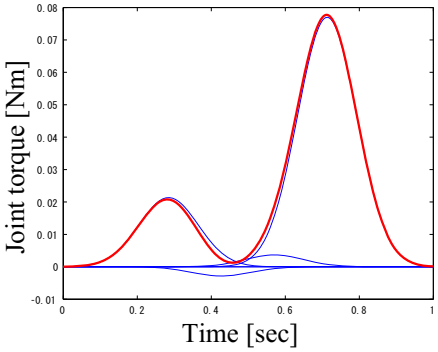

(d) Obtained joint torque

Figure 12: Throw C

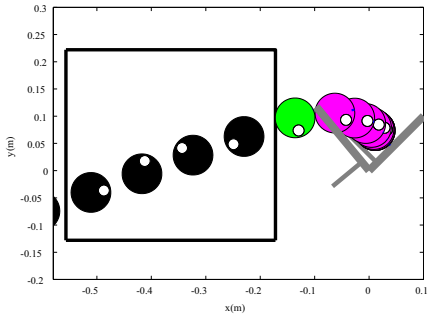

(a) Simulation

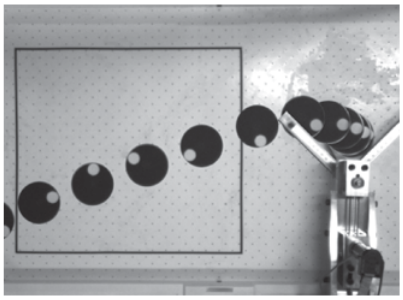

(b) Experiment

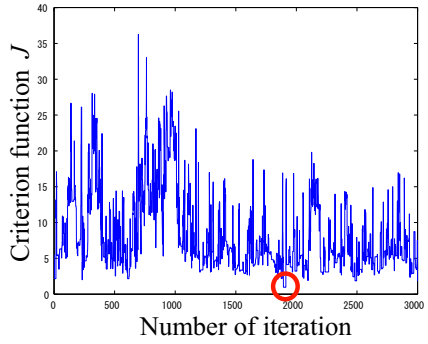

(c) Simulated Annealing

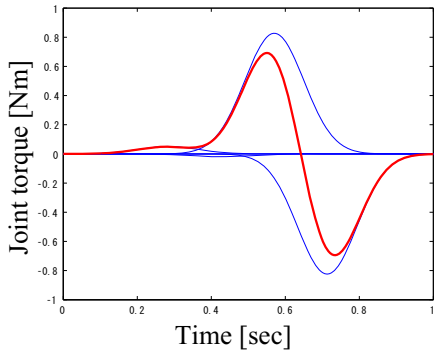

(d) Obtained joint torque

Figure 13: Throw D

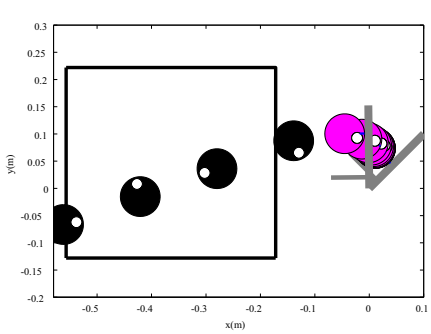

(a) Simulation

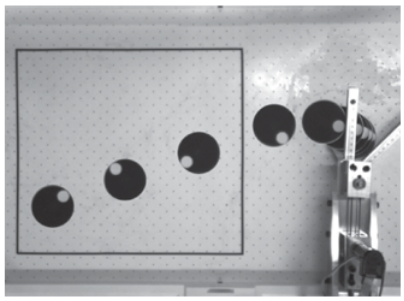

(b) Experiment

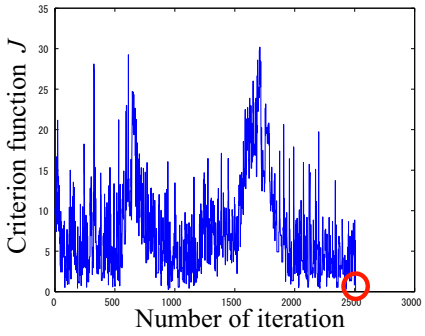

(c) Simulated Annealing

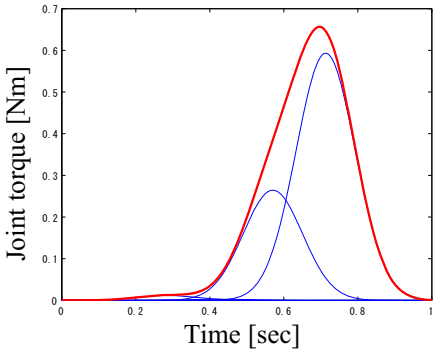

(d) Obtained joint torque

Figure 14: Throw E

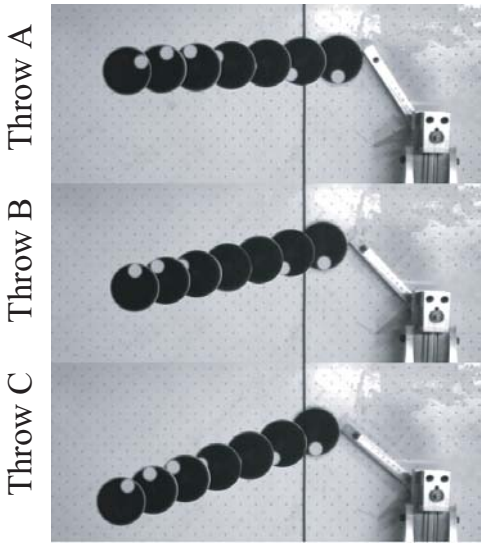

Figure 15: Throwing in the same velocity, but in different directions: Throws A to C

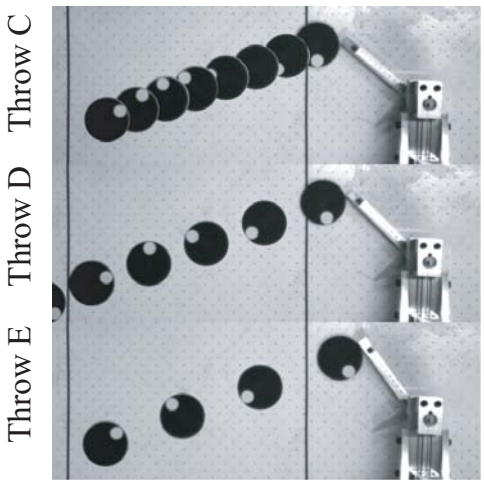

Figure 16: Throwing in the same direction, but in different velocities: Throws C to E

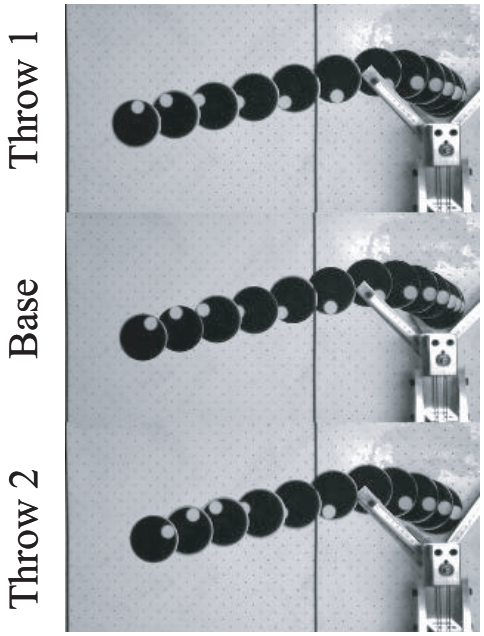

Figure 17: Throwing in the same direction and angular velocity, but in different velocities

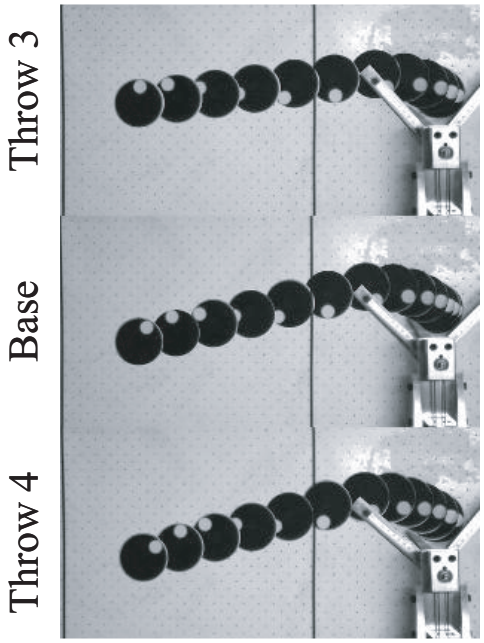

Figure 18: Throwing in the same velocity and angular velocity, but in different directions

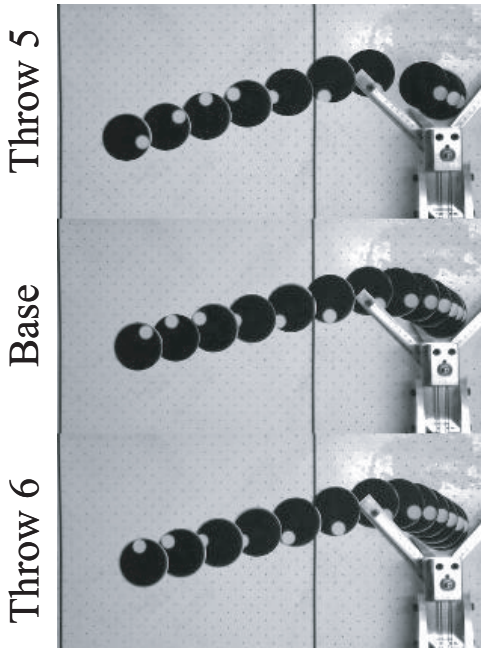

Figure 19: Throwing in the same velocity and direction, but in different angular velocities

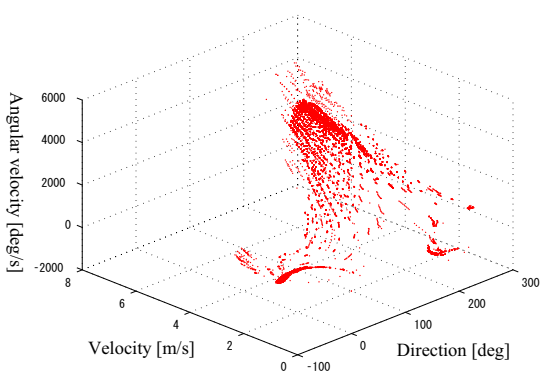

(a) Search Result

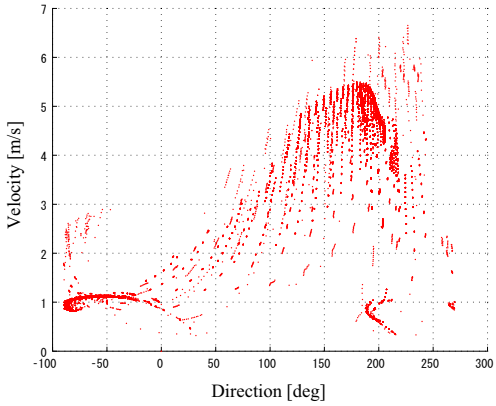

(b) Velocity-Direction

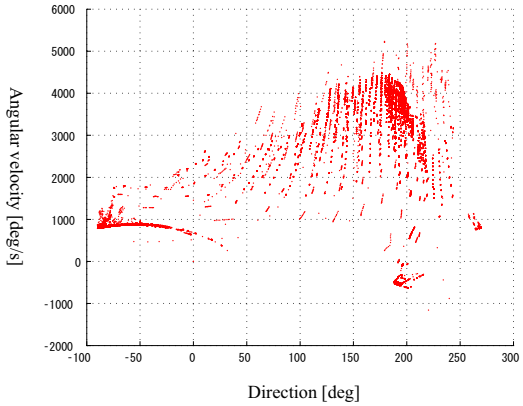

(c) Angular velocity-Direction

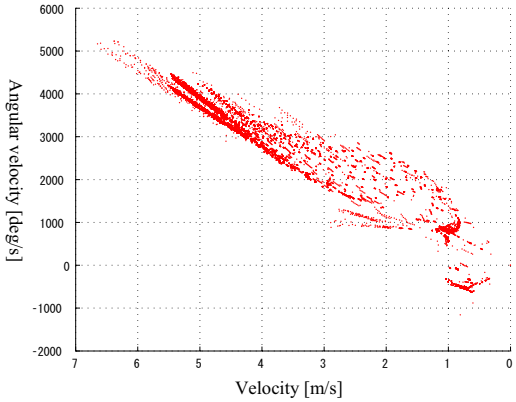

(d) Angular velocity-Velocity

Figure 20: Result of Global Search for Vertical Throwing

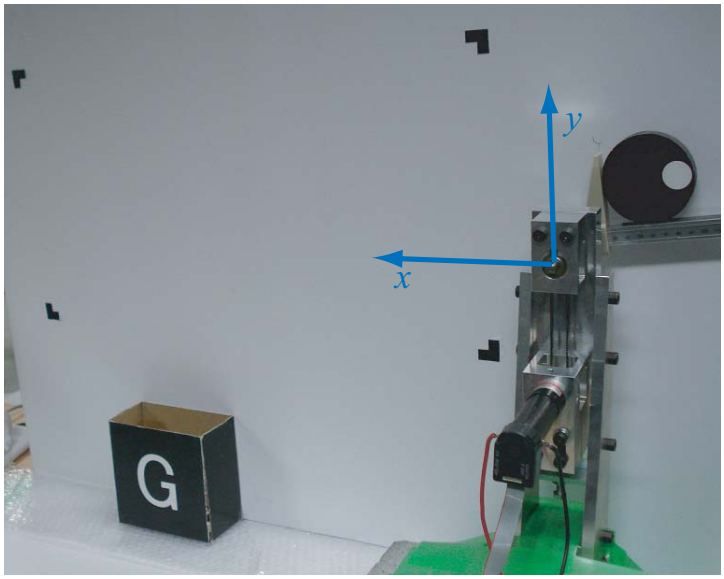

Figure 21: Experimental System for Vertical Throwing

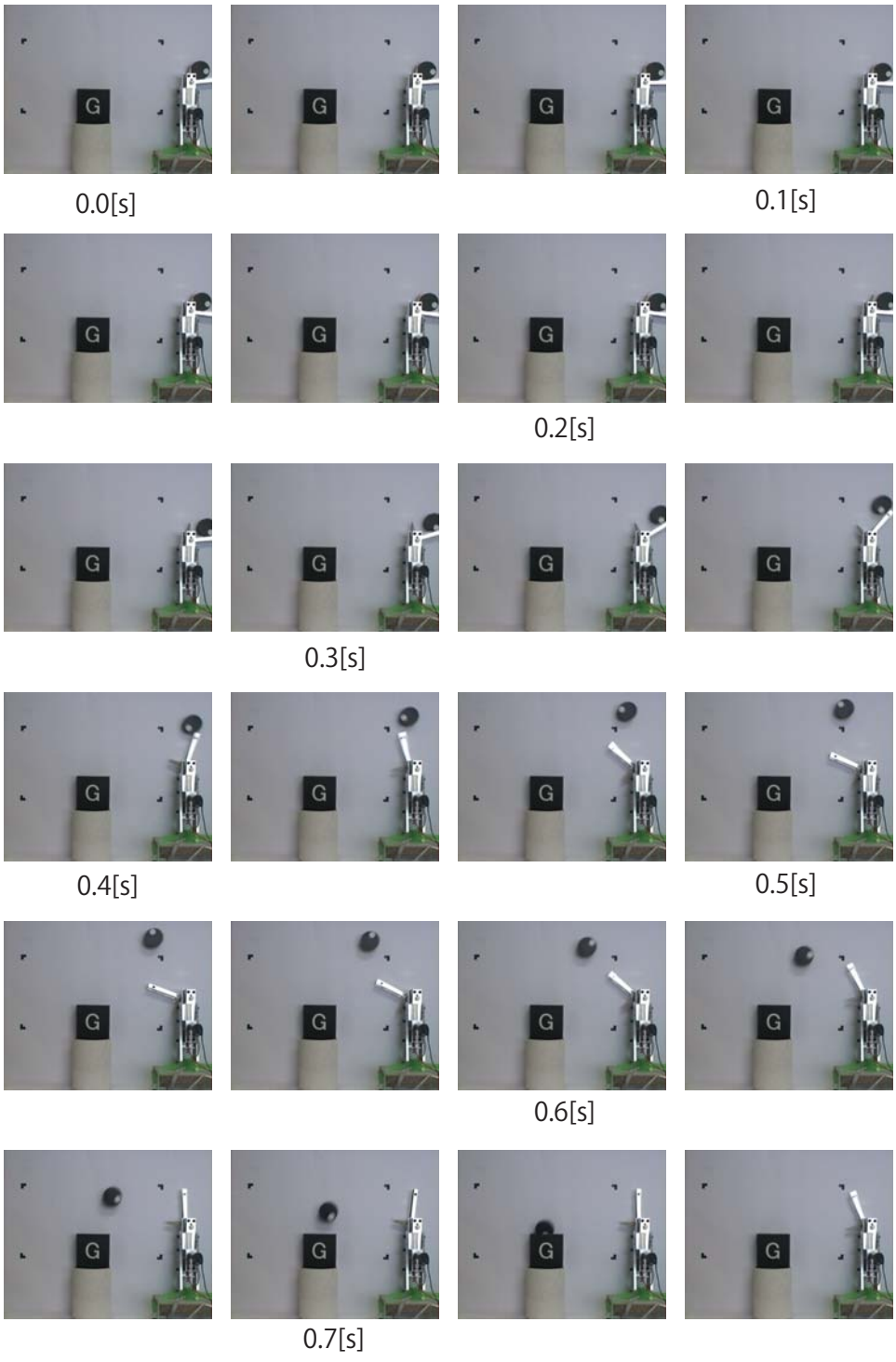

Figure 22: Throwing in the Vertical Plane: Throw $V1$

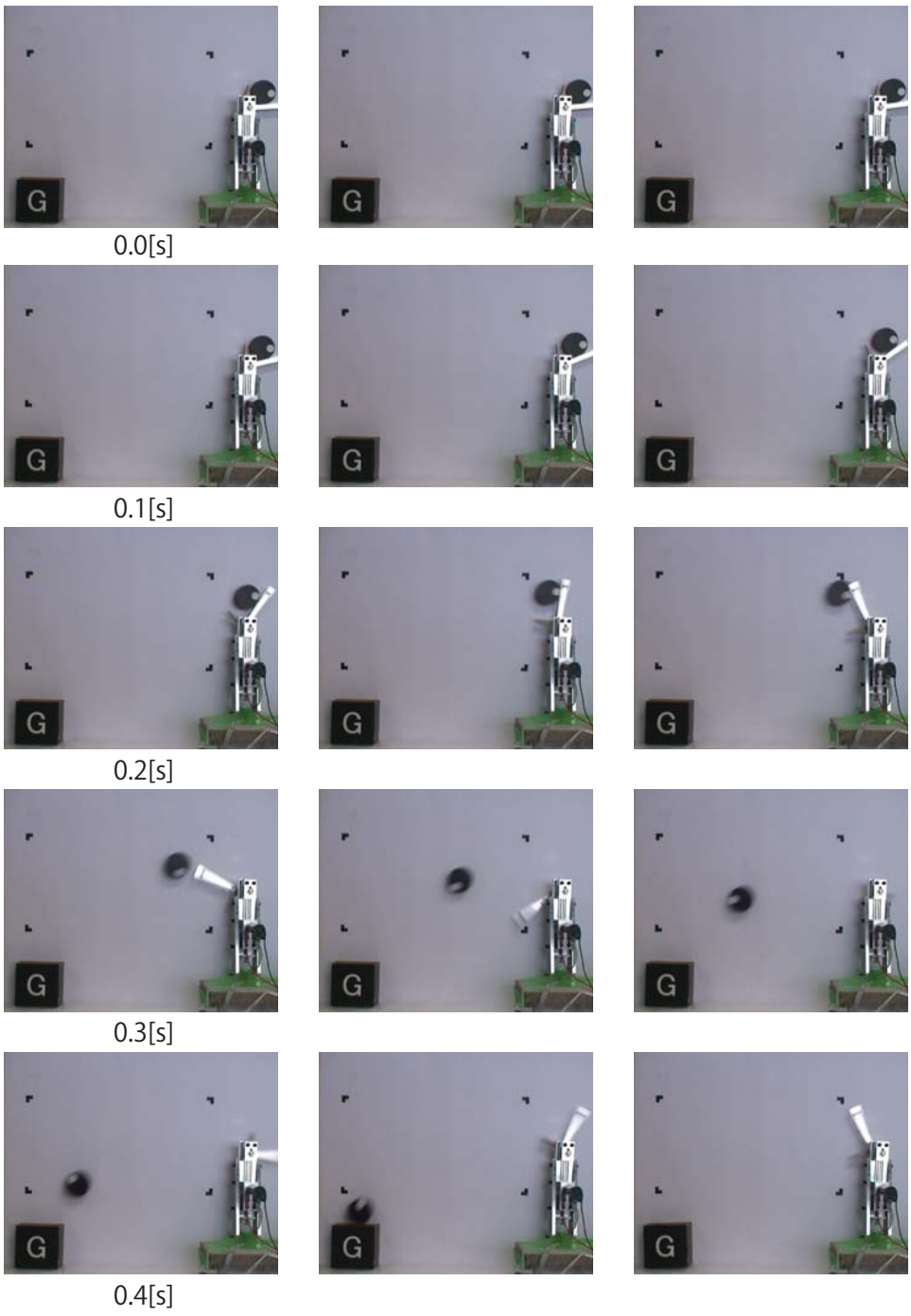

Figure 23: Throwing in the Vertical Plane: Throw $V2$